Enhanced DR Screening Using DiabDHS-Net: A Deep Learning Approach with FGK Clustering and Morphological Processing

Fahimuddin Shaik
Department of Electronics and Communication Engineering, Annamacharya University, Rajampet, Andhra Pradesh, India
fahimaits@gmail.com (corresponding author)

Pravin Ramdas Kshirsagar
Department of Electronics and Telecommunication Engineering, J.D.College of Engineering & Management, Nagpur, India
pravinrk88@yahoo.com

Sivaneasan Bala Krishnan
Engineering Cluster, Singapore Institute of Technology, 10 Dover Drive, Singapore
sivaneasan@singaporetech.edu.sg

Vijaya Krishna Akula
Department of Information Technology, G. Narayanamma Institute of Technology and Science for Women, Hyderabad, India
vijayakrishnaakula2022@gnits.ac.in

Shrikant Vijayrao Sonekar
Department of Computer Science & Engineering, J. D. College of Engineering & Management, Nagpur, India
principal@jdcoem.ac.in

Ramakantha B. Reddy
Department of CSE (AIML), Sri Venkateswara College of Engineering, Tirupati, Andhra Pradesh, India
ramakanthareddy@gmail.com

Received: 1 June 2025 | Revised: 1 July 2025 and 16 July 2025 | Accepted: 20 July 2025

 DOI: https://doi.org/10.48084/etasr.12496

ABSTRACT

Diabetic Retinopathy (DR) develops as a microvascular diabetes complication that affects the retinal blood vessels and causes vision loss that could become permanent unless diagnosed and treated appropriately. Research on deep learning-based detection of DR has gained extensive popularity due to improvements in medical image processing and neural network designs. The DiabDHS-Net model uses DenseNet201 with the Human Evolutionary Optimization Algorithm (HEOA) and Softmax classifier for automated DR detection. The novelty of this model is that DenseNet extracts dense features with maximum information retention, and HEOA optimizes networks to find distant global solutions suitable for medical applications. The identification process for the fovea region depends on FGK Clustering (Fuzzy Gustafson-Kessel) to achieve high accuracy results. Experimental investigation in the Messidor dataset demonstrates that the proposed model surpasses existing models by achieving 99.53% accuracy, 99.12% precision, 99.67% recall, and 98.9% F1-score, along with 99.81% specificity. ROC curve and feature importance plots prove that the model distinguishes different DR severity levels (No DR, Mild DR, Moderate DR, Severe DR) with high levels of sensitivity and specificity.

Keywords-segmentation; medical devices; IoMT; healthcare; accuracy; precision

I. INTRODUCTION

The complication of microvascular disease known as DR progressively reacts to diabetes, causing damage to the retinal blood vessels and eventually impaired vision and blindness at the final stage [1-3]. DR has become the dominant preventable cause of blindness because the prevalence of diabetes worldwide continues to increase and mostly affects people between working ages. The disease moves from non-proliferative DR through several stages, until it turns into severe proliferative DR that includes abnormal blood vessel growth and hemorrhages [4-8]. Early identification of microaneurysms along with hemorrhages, exudates, and neovascularization in the retina requires immediate treatment and intervention [9]. Standard clinical examinations of the eyes through fundus imaging, together with fluorescein angiography, require skilled interpretation. However, such an analysis often takes a significant amount of time while showing variability between different observers [10-15].

Early detection of DR is critical, as the disease is often asymptomatic in its early stages [16-18]. If left untreated, it can result in irreversible vision loss due to retinal detachment or macular edema [19-21]. Early intervention with laser photocoagulation, anti-VEGF therapy, or vitrectomy can significantly reduce the risk of vision impairment [22-25]. The key contributions of this work include the development of DiabDHS-Net, an optimized deep learning model that integrates DenseNet201, the Human Evolutionary Optimization Algorithm (HEOA), and a softmax classifier for effective DR classification. A user-friendly GUI was created to facilitate the entire diagnostic process, including image acquisition, preprocessing, segmentation, feature extraction, and classification. Fovea localization was improved using Fuzzy Gustafson-Kessel (FGK) clustering to improve region-based feature extraction.

II. RELATED WORKS

In [26], the RSG-Net model was proposed to classify DR into four classes. However, models with a heavy reliance on convolutional layers raise computational demands, potentially limiting deployment in environments with limited hardware resources. In [27], EfficientNet was used to diagnose DR, but its architectural complexity, while contributing to its high performance, requires extensive computational resources, which may be a limiting factor in resource-constrained environments. In [28], EfficientNetB0 was used for the same purpose. The challenge with EfficientNetB0 is its sensitivity to hyperparameter settings, which can complicate the model's application across diverse datasets without significant tuning. In [29], a CNN was customized to enable targeted feature learning. However, such approaches may not generalize well across different types of DR, limiting their use in broader clinical applications.

In [30], VGG Net was used, with its extensive architecture resulting in high computational load and slower inference times, making it unsuitable for real-time analysis. In [31], DenseNet121 was used, as its depth enables robust feature extraction, but at the expense of increased computational demands, particularly during training and operational deployment. In [32], a basic CNN was used with ADAM optimization, which was less computationally demanding but may lack the depth needed to effectively capture complex patterns, limiting its efficacy. In [33], a hybrid deep learning model combined Histogram Gradient Boosting (HGB) and Support Vector Machines (SVM). The use of multiple models in a hybrid approach adds complexity and may present difficulties in model tuning and data preprocessing.

III. PROPOSED SYSTEM

The proposed method for detecting DR, as shown in Figure 1, utilizes a comprehensive process that incorporates a GUI for medical image processing. It integrates the FGK clustering algorithm for exact region of interest (fovea) identification, morphological operations for feature enhancement, and an advanced classification model, DiabDHS-Net, including evolutionary optimization. Initially, retinal images are loaded from a dedicated database into the GUI. These images are then standardized to uniform dimensions to facilitate consistent analysis.

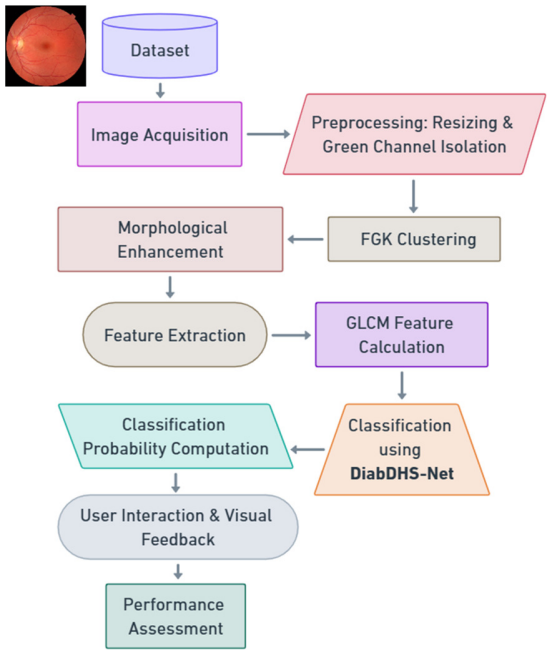

Fig. 1. Block diagram of the proposed method.

A. Preprocessing

All retinal images were resized to a uniform dimension using bilinear interpolation and normalized between [0,1] to ensure uniform pixel distribution. Contrast enhancement and noise reduction were applied to improve vessel visibility and feature extraction quality.

$$I_{resized} = resize\left(I_{original}, new\_width, new\_height\right) \quad (1)$$

where $I_{original}$ is the original image matrix, and new_width and new_height are the dimensions of the resized image.

$$I_{green} = I_{original}[:, :2] \quad (2)$$

where I_{green} represents the green channel of the image.

The fovea is identified as the region of interest using the FGK clustering algorithm, which allows flexible membership degrees [34]. FGK clustering dynamically adjusts the shape of each cluster using an adaptive covariance matrix, making it highly suitable for fovea detection where elliptical structures dominate.

$$J(U,V) = \sum_{i=1}^{c}\sum_{k=1}^{n} u_{ik}^{m}\|x_k - v_i\|_A^2 \quad (3)$$

where U represents the membership matrix,V represents the centers matrix, u_{ik} represents the membership degree of data point k in cluster i, x_k represents a data point, v_i represents the center of cluster i, A represents the covariance matrix adjusting the distance metric, c is the number of clusters, n represents the number of data points, and m represents the fuzziness parameters.

Morphological operations such as dilation and erosion are applied to enhance the visibility of specific retinal structures.

$$I_{dilated} = I \oplus B \quad (4)$$

where $I_{dilated}$ represents the image after dilation, I represents the input image, and B represents the structured element used for dilation

$$I_{eroded} = I \ominus B \quad (5)$$

where I_{eroded} represents the image after erosion

Statistical and textural features are extracted to characterize the region effectively.

$$M = \frac{1}{N}\sum_{i=1}^{N} I_i \quad (6)$$

where M represents the mean intensity of the region, I_i represents the intensity value of the i^{th} pixel, and N represents the total number of pixels in the region

$$H = -\sum_{i=1}^{L} p(i) log p(i) \quad (7)$$

where H represents the entropy of the region, $p(i)$ represents the probability of occurrence of the i^{th} intensity level, and L represents the number of possible intensity levels

$$Contrast = \sum_{i,j}(i-j)^2 P(i,j) \quad (8)$$

$$Correlation = \frac{\sum_{i,j}(i-\mu_i)(i-\mu_j)P(i,j)}{\sigma_i \sigma_j} \quad (9)$$

$$Energy = \sum_{i,j} P(i,j)^2 \quad (10)$$

$$Homogeneity = \sum_{i,j} \frac{P(i,j)}{1+|i-j|} \quad (11)$$

where $P(i,j)$ represents the co-occurrence matrix probability value for pixel intensities, and μ and σ represent the mean and standard deviation of the intensities.

The extracted features are classified using the DiabDHS-Net model, which includes evolutionary optimization. The population initialization is given by

$$x_i = \alpha \cdot x_{i-1} \cdot (1 - x_{i-1}) \quad (12)$$

$$x_{0i} = lb + (ub - lb) \cdot x_i \quad (13)$$

where x_i represents the position of the i^{th} individual in the population, α represents the logistic map parameter, and ub and lb represent the lower and upper bounds of the search space. HEOA mimics human decision evolution using chaotic population initialization and iterative improvement strategies, making it effective for selecting high-impact features in complex medical datasets.

$$X_{t+1,i} = \beta \cdot \left(1 - \frac{t}{MaxIter}\right) \cdot \left(X_{t,i} - X_{best}\right) \cdot Levy(dim) + X_{best} \cdot \left(1 - \frac{t}{MaxIter}\right) + \left(X_{t,mean} - X_{best}\right) \cdot floor(rand \cdot jump).jump \quad (14)$$

where $X_{t,i}$ represents the current position of the i^{th} individual, X_{best} represents the best position found so far, and $MaxIter$ represents the maximum number of iterations.

$$P(y = k|x) = \frac{e^{x^T \beta_k}}{\sum_{j=1}^{k} e^{x^T \beta_k}} \quad (15)$$

where $P(y = k|x)$ represents the probability of the class k given features, and β_k represents coefficients for class k

Performance evaluation is carried out using:

$$Accuracy = \frac{(TP + TN)}{(TP + TN + FP + FN)} \quad (16)$$

$$Specificity = \frac{TN}{(TN + FP)} \quad (17)$$

$$Recall\ (Sensitivity) = \frac{TP}{TP + FN} \quad (18)$$

B. Proposed Model

The deep learning architecture DiabDHS-Net, shown in Figure 2, serves medical image classification to identify DR in diagnosis processes. The network structure unites DenseNet 201 with HEOA and a softmax classifier.

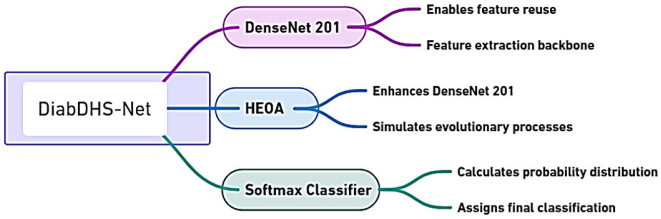

Fig. 2. Diagram of the proposed DiabDHS-Net.

C. Algorithm of DiabDHS-Net Model Architecture:

The algorithm below details each step of the process, from initialization to classification, for deep learning and optimization implementation.

```
Algorithm of the proposed DiabDHS-Net
Architecture
1. Initialize:
   Load DenseNet201
   Set HEOA parameters: alpha, lb, ub,
   MaxIter
2. Preprocess Image:
   Input retinal image
   Resize and normalize
3. Extract Features:
   Pass the image through DenseNet201
   Concatenate features from key layers
4. Optimize Features (HEOA):
   Initialize population with features
   Apply chaotic mapping:
   For iter = 1 to MaxIter:
     Evaluate fitness,
     Apply selection, crossover, mutation
5. Classify:
   Input optimized features to softmax
   Predict the class with the highest
   probability
6. Output:
   Return predicted class and confidence
   Optionally show feature maps and logs
```

IV. RESULTS AND DISCUSSION

The Messidor dataset was created to help researchers with computer-aided diagnosis (CAD) of DR [25]. It includes 1,200 retinal fundus images obtained from three ophthalmologic departments. The dataset assigns a Retinopathy Grade (0-3) based on the severity of the DR. Since 1,200 images are insufficient for deep learning models, the dataset was augmented to 100,000 images using various techniques based on the prevalence of severity levels of DR. The severity labels for DR (No DR, Mild, Moderate, Severe) were adopted from the Messidor dataset's reference annotations, which are based on clinical retinal grading protocols. The distribution of the dataset is shown in Table I and Figure 3.

TABLE I. DATASET DISTRIBUTION AND SPLIT

Retinopathy grade	Total images	Split (Train/Val/Test)
0 - No DR	20,000	14,000/2,000/4,000
1 - Mild DR	20,000	14,000/2,000/4,000
2 - Moderate DR	25,000	17,500/2,500/5,000
3 - Severe DR	35,000	24,500/3,500/7,000
Total	**100,000**	**70,000/10,000/20,000**

Figure 4 shows a retinal fundus image derived from a non-mydriatic fundus camera [25]. The conversion of the image to grayscale, as shown in Figure 5, serves as a requirement for feature extraction procedures. Figure 6 depicts the enhanced image, which was created using contrast adjustments and noise reduction.

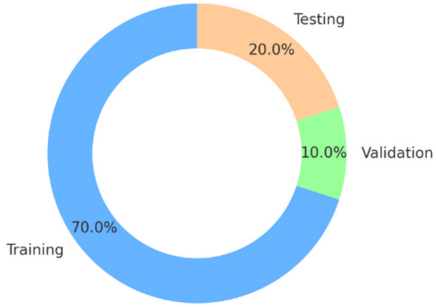

Fig. 3. Overall dataset distribution chart.

Fig. 4. Retinal fundus image.

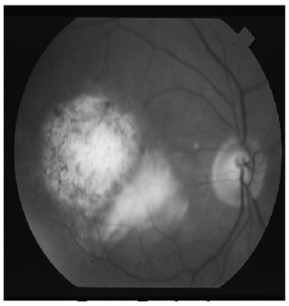

Fig. 5. Grayscale image.

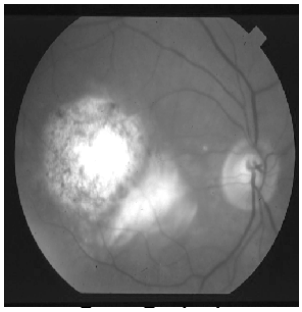

Fig. 6. Enhanced image.

Morphological operations were then performed. Figure 7 shows the dilated image, where dilation expands bright regions, making vessels and lesions more visible. Figure 8 depicts the eroded image, in which erosion reduces unwanted noise and removes small artifacts. In Figure 9, the difference image is created by subtracting the eroded image from the dilated image. Blood vessel segmentation comes next, as shown in Figure 10, where blood vessel detection is successfully extracted.

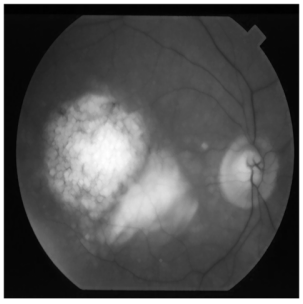

Fig. 7. Dilated image.

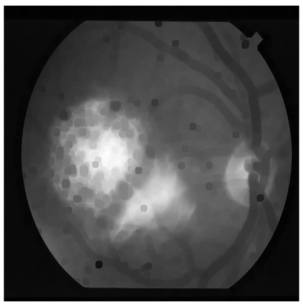

Fig. 8. Eroded image.

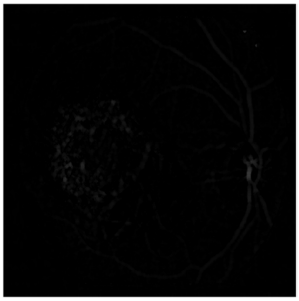

Fig. 9. Difference image.

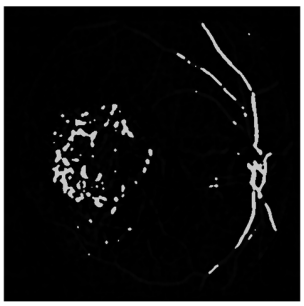

Fig. 10. Blood vessel detection.

After blood vessel extraction, the thinning operation is performed, resulting in the refined vascular map, as shown in Figure 11. Single pixel width simplification of vessel structures during this step maintains topological accuracy by removing extra pixels. Figure 12 represents the final retinal vessel detection image, demonstrating the processed retinal vascular network that reveals key areas of capillary dropout.

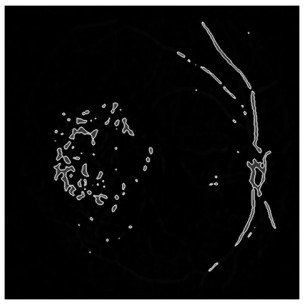

Fig. 11. Thinning operation.

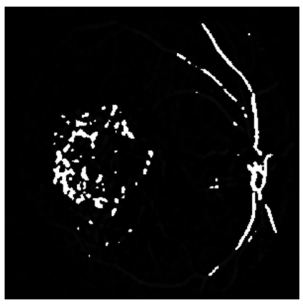

Fig. 12. Vessel detection.

Table II shows an accuracy comparison, where the proposed model outperforms the previous best-performing model, RSG-Net (99.36%) [26]. Figure 13 depicts this comparison graphically.

TABLE II. ACCURACY COMPARISON

Model	Accuracy (%)
RSG-Net [26]	99.36
EfficientNet [27]	94
EfficientNetB0 [28]	91
Customized CNN [29]	90
VGG Net [30]	97
DenseNet121 [31]	96.11
Basic CNN with ADAM optimizer [32]	71.85
Hybrid DL (HGB + SVM) [33]	96.9
Proposed model	**99.53**

Table III focuses on precision, which is an important indicator of how many of the identified positive cases are correct. The proposed model achieved a precision of 99.12%, outperforming others. Figure 14 shows a visual comparison, demonstrating the proposed model's effectiveness in making accurate positive predictions. Table V and Figure 16 compare F1-scores, a balanced metric that takes into account both precision and recall. The proposed model achieved an F1-score of 98.9%, outperforming all other models.

TABLE III. PRECISION

Model	Precision (%)
EfficientNet [27]	87
EfficientNetB0 [28]	97.03
Customized CNN [29]	88
VGG Net [30]	95
Basic CNN with ADAM optimizer [32]	72
Hybrid Deep Learning (HGB + SVM) [33]	96.9
Proposed Model	**99.12**

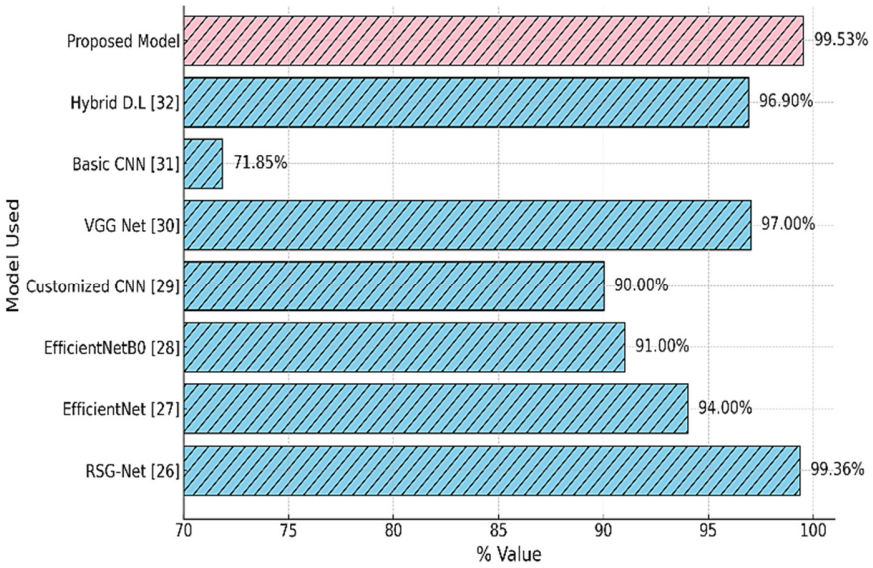

Fig. 13. Accuracy comparison plot.

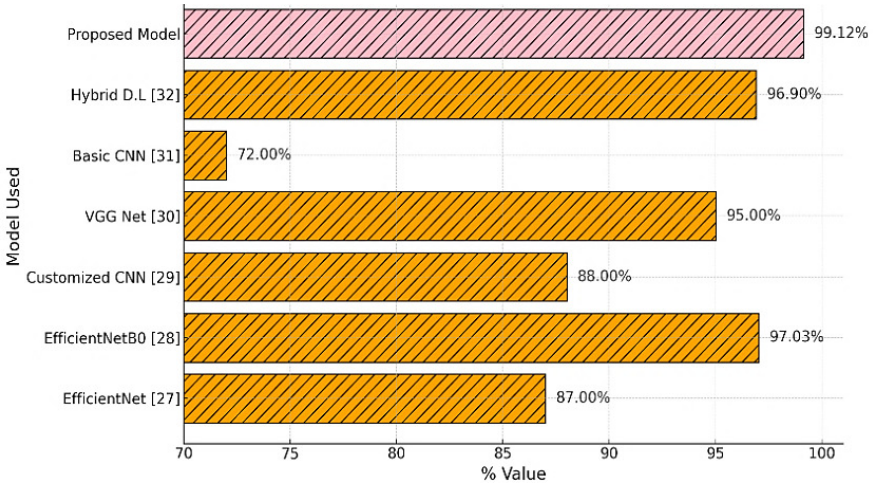

Fig. 14. Precision comparison plot

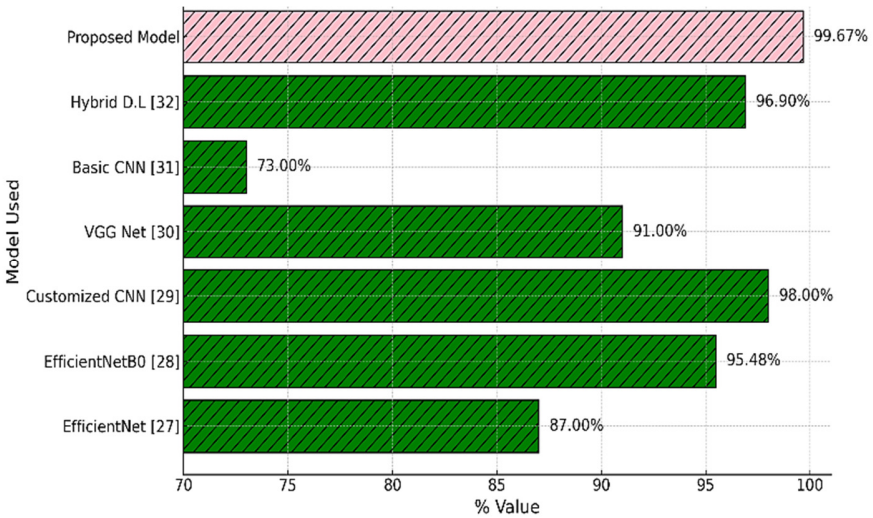

Fig. 15. Recall comparison plot.

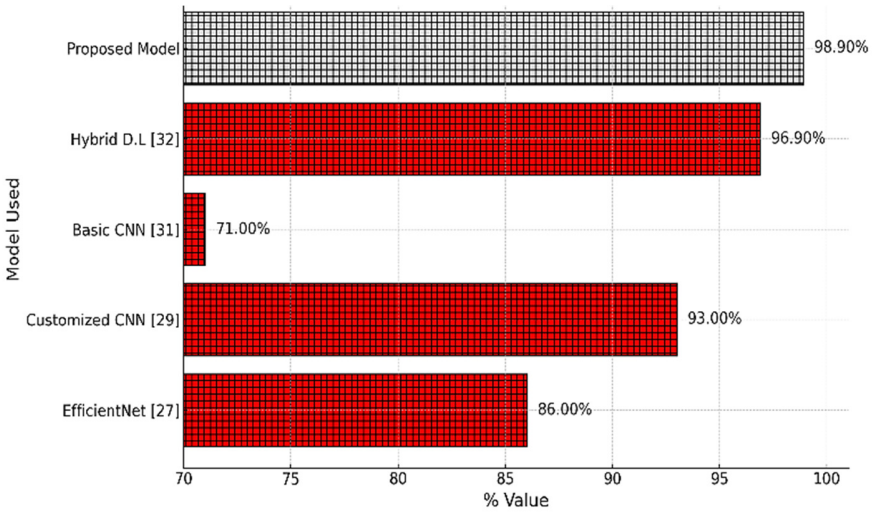

Fig. 16. F1-score comparison plot.

TABLE IV. RECALL COMPARISON

Model	Recall (%)
EfficientNet [27]	87
EfficientNetB0 [28]	95.48
Customized CNN [29]	98
VGG Net [30]	91
Basic CNN with ADAM optimizer [32]	73
Hybrid Deep Learning (HGB + SVM) [33]	96.9
Proposed Model	99.67

TABLE V. F1-SCORE COMPARISON

Model	F1-score (%)
EfficientNet [27]	86
Customized CNN [29]	93
Basic CNN with ADAM optimizer [32]	71
Hybrid Deep Learning (HGB + SVM) [33]	96.9
Proposed Model	98.9

Table VI compares specificity, which measures how well each model correctly identifies negative cases. The proposed model achieved the highest specificity at 99.81%. Figure 17 depicts the specificity comparisons, demonstrating the proposed model's ability to accurately exclude negative cases.

TABLE VI. SPECIFICITY COMPARISON

Model	Specificity (%)
RSG-Net [26]	99.79
Proposed Model	99.81

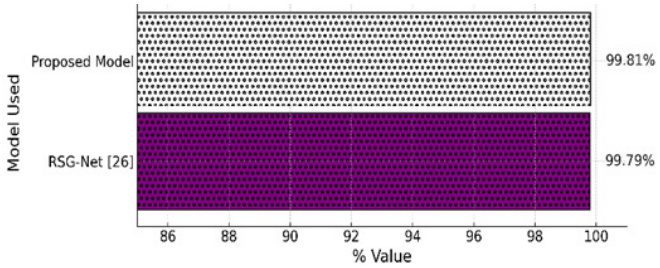

Fig. 17. Specificity comparison plot.

As shown in Figure 18, the ROC-AUC scores achieved for each class were: No DR 0.963, Mild DR 0.945, Moderate DR 0.954, and Severe DR 0.935.

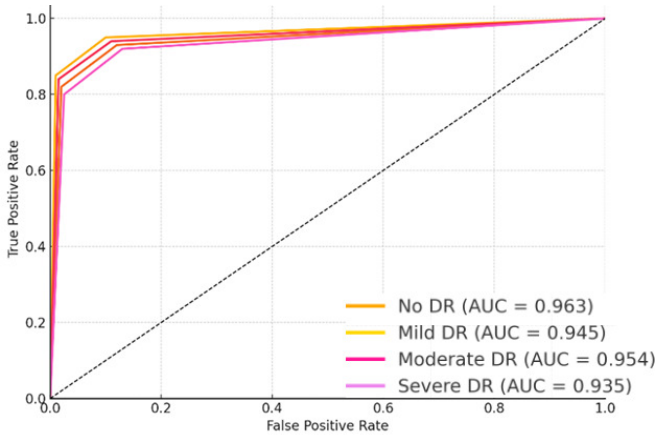

Fig. 18. ROC curves and AUC for DR severity levels.

These high ROC-AUC values confirm the effectiveness of the model in distinguishing between DR severity levels. DiabDHS-Net has strong potential for integration into clinical screening programs and teleophthalmology platforms. Its ability to automatically detect the severity levels of DR with high precision can assist clinicians in early diagnosis, reduce the screening workload, and support remote real-time consultations in underserved regions.

V. CONCLUSION

The DiabDHS-Net model combines DenseNet201, HEOA, and a softmax classifier to effectively address automated DR detection, providing high classification accuracy. Built within a MATLAB-based GUI, the system streamlines image acquisition, preprocessing, segmentation, and fovea localization using FGK clustering, while enhancing blood vessel visibility through morphological operations. Trained on

a robust 100,000-image dataset, derived from augmented Messidor images, the model handles variations in lighting, orientation, and capture conditions. The proposed model achieved excellent performance with 99.53% accuracy, 99.12% precision, 99.67% recall, 98.9% F1-score, and 99.81% specificity, outperforming models such as RSG-Net, EfficientNet, and hybrid deep learning approaches. ROC-AUC curves and feature importance analyses further confirm its effectiveness across DR severity levels, making it suitable for telemedicine applications. The model balances computational efficiency and predictive accuracy, addressing key limitations of current solutions.

ACKNOWLEDGEMENT

This work was carried out as part of a Post-Doctoral Research (Remote) at the Singapore Institute of Technology (SIT). The authors acknowledge the SIT for supporting this Post-Doctoral Research (Remote).

REFERENCES

[1] E. AbdelMaksoud, S. Barakat, and M. Elmogy, "A computer-aided diagnosis system for detecting various diabetic retinopathy grades based on a hybrid deep learning technique," *Medical & Biological Engineering & Computing*, vol. 60, no. 7, pp. 2015–2038, Jul. 2022, https://doi.org/10.1007/s11517-022-02564-6.

[2] Padmanayana and B. K. Anoop, "Binary Classification of DR-Diabetic Retinopathy using CNN with Fundus Colour Images," *Materials Today: Proceedings*, vol. 58, pp. 212–216, 2022, https://doi.org/10.1016/j.matpr.2022.01.466.

[3] N. Barhate, S. Bhave, R. Bhise, R. G. Sutar, and D. C. Karia, "Reducing Overfitting in Diabetic Retinopathy Detection using Transfer Learning," in *2020 IEEE 5th International Conference on Computing Communication and Automation (ICCCA)*, Greater Noida, India, Oct. 2020, pp. 298–301, https://doi.org/10.1109/ICCCA49541.2020.9250772.

[4] K. Sangeetha, K. Valarmathi, T. Kalaichelvi, and S. Subburaj, "A broad study of machine learning and deep learning techniques for diabetic retinopathy based on feature extraction, detection and classification," *Measurement: Sensors*, vol. 30, Dec. 2023, Art. no. 100951, https://doi.org/10.1016/j.measen.2023.100951.

[5] T. E. Rohan, C. D. Frost, and N. J. Wald, "Prevention of blindness by screening for diabetic retinopathy: a quantitative assessment.," *British Medical Journal*, vol. 299, no. 6709, pp. 1198–1201, Nov. 1989, https://doi.org/10.1136/bmj.299.6709.1198.

[6] F. L. Ferris III, "How Effective Are Treatments for Diabetic Retinopathy?," *JAMA*, vol. 269, no. 10, pp. 1290–1291, Mar. 1993, https://doi.org/10.1001/jama.1993.03500100088034.

[7] B. Antal and A. Hajdu, "An ensemble-based system for automatic screening of diabetic retinopathy," *Knowledge-Based Systems*, vol. 60, pp. 20–27, Apr. 2014, https://doi.org/10.1016/j.knosys.2013.12.023.

[8] R. Ramesh and S. Sathiamoorthy, "A Deep Learning Grading Classification of Diabetic Retinopathy on Retinal Fundus Images with Bio-inspired Optimization," *Engineering, Technology & Applied Science Research*, vol. 13, no. 4, pp. 11248–11252, Aug. 2023, https://doi.org/10.48084/etasr.6033.

[9] A. Hutchinson *et al.*, "Effectiveness of screening and monitoring tests for diabetic retinopathy – a systematic review," *Diabetic Medicine*, vol. 17, no. 7, pp. 495–506, 2000, https://doi.org/10.1046/j.1464-5491.2000.00250.x.

[10] J. K. H. Goh, C. Y. Cheung, S. S. Sim, P. C. Tan, G. S. W. Tan, and T. Y. Wong, "Retinal Imaging Techniques for Diabetic Retinopathy Screening," *Journal of Diabetes Science and Technology*, vol. 10, no. 2, pp. 282–294, Mar. 2016, https://doi.org/10.1177/1932296816629491.

[11] V. Sathananthavathi and G. Indumathi, "Deep learning approaches for the retinal vasculature segmentation in fundus images," in *Computational Methods and Deep Learning for Ophthalmology*, Elsevier, 2023, pp. 139–155.

[12] N. Tsiknakis *et al.*, "Deep learning for diabetic retinopathy detection and classification based on fundus images: A review," *Computers in Biology and Medicine*, vol. 135, Aug. 2021, Art. no. 104599, https://doi.org/10.1016/j.compbiomed.2021.104599.

[13] D. Doshi, A. Shenoy, D. Sidhpura, and P. Gharpure, "Diabetic retinopathy detection using deep convolutional neural networks," in *2016 International Conference on Computing, Analytics and Security Trends (CAST)*, Pune, India, Dec. 2016, pp. 261–266, https://doi.org/10.1109/CAST.2016.7914977.

[14] G. T. Zago, R. V. Andreão, B. Dorizzi, and E. O. Teatini Salles, "Diabetic retinopathy detection using red lesion localization and convolutional neural networks," *Computers in Biology and Medicine*, vol. 116, Jan. 2020, Art. no. 103537, https://doi.org/10.1016/j.compbiomed.2019.103537.

[15] S. N. Firke and R. B. Jain, "Convolutional Neural Network for Diabetic Retinopathy Detection," in *2021 International Conference on Artificial Intelligence and Smart Systems (ICAIS)*, Coimbatore, India, Mar. 2021, pp. 549–553, https://doi.org/10.1109/ICAIS50930.2021.9395796.

[16] A. Gamal Eldin, M. Mustafa, R. Eltayeb, and F. Mohamed, "Automatic Detection of Diabetic Retinopathy using Neural Networks and Support Vector Machine," in *2020 International Conference on Computing and Information Technology (ICCIT-1441)*, Tabuk, Saudi Arabia, Sep. 2020, pp. 1–5, https://doi.org/10.1109/ICCIT-144147971.2020.9213746.

[17] Y. Xie *et al.*, "Artificial intelligence for teleophthalmology-based diabetic retinopathy screening in a national programme: an economic analysis modelling study," *The Lancet Digital Health*, vol. 2, no. 5, pp. e240–e249, May 2020, https://doi.org/10.1016/S2589-7500(20)30060-1.

[18] S. A. Hassan, S. Akbar, A. Rehman, T. Saba, H. Kolivand, and S. A. Bahaj, "Recent Developments in Detection of Central Serous Retinopathy Through Imaging and Artificial Intelligence Techniques–A Review," *IEEE Access*, vol. 9, pp. 168731–168748, 2021, https://doi.org/10.1109/ACCESS.2021.3108395.

[19] S. Riaz, T. Jahangir, and T. Khan, "Frequency of Diabetic Retinopathy and Factors for Suboptimal Diabetic Control in Type 2 Diabetic Patients in a Trust Hospital of Pakistan," *Pakistan Journal of Ophthalmology*, vol. 37, no. 2, Jan. 2021, https://doi.org/10.36351/pjo.v37i2.1123.

[20] V. Gulshan *et al.*, "Development and Validation of a Deep Learning Algorithm for Detection of Diabetic Retinopathy in Retinal Fundus Photographs," *JAMA*, vol. 316, no. 22, Dec. 2016, Art. no. 2402, https://doi.org/10.1001/jama.2016.17216.

[21] X. Li, T. Pang, B. Xiong, W. Liu, P. Liang, and T. Wang, "Convolutional neural networks based transfer learning for diabetic retinopathy fundus image classification," in *2017 10th International Congress on Image and Signal Processing, BioMedical Engineering and Informatics (CISP-BMEI)*, Shanghai, China, Oct. 2017, pp. 1–11, https://doi.org/10.1109/CISP-BMEI.2017.8301998.

[22] M. Arora and M. Pandey, "Deep Neural Network for Diabetic Retinopathy Detection," in *2019 International Conference on Machine Learning, Big Data, Cloud and Parallel Computing (COMITCon)*, Faridabad, India, Feb. 2019, pp. 189–193, https://doi.org/10.1109/COMITCon.2019.8862217.

[23] R. Revathy, B. S. Nithya, J. J. Reshma, S. S. Ragendhu, and M. D. Sumithra, "Diabetic Retinopathy Detection using Machine Learning," *International Journal of Engineering Research and*, vol. V9, no. 06, Jun. 2020, Art. no. IJERTV9IS060170, https://doi.org/10.17577/IJERTV9IS060170.

[24] S. El-Ateif and A. Idri, "Single-modality and joint fusion deep learning for diabetic retinopathy diagnosis," *Scientific African*, vol. 17, Sep. 2022, Art. no. e01280, https://doi.org/10.1016/j.sciaf.2022.e01280.

[25] E. Decencière *et al.*, "Feedback on a publicly distributed database: the Messidor database," *Image Analysis & Stereology*, vol. 33, no. 3, Aug. 2014, Art. no. 231, https://doi.org/10.5566/ias.1155.

[26] S. Akhtar *et al.*, "A deep learning based model for diabetic retinopathy grading," *Scientific Reports*, vol. 15, no. 1, Jan. 2025, Art. no. 3763, https://doi.org/10.1038/s41598-025-87171-9.

[27] R. H. Abood and A. H. Hamad, "Multi-Label Diabetic Retinopathy Detection Using Transfer Learning Based Convolutional Neural Network," *Fusion: Practice and Applications*, vol. 17, no. 2, pp. 279–293, 2025, https://doi.org/10.54216/FPA.170221.

[28] V. Anand, D. Koundal, W. Y. Alghamdi, and B. M. Alsharbi, "Smart grading of diabetic retinopathy: an intelligent recommendation-based fine-tuned EfficientNetB0 framework," *Frontiers in Artificial Intelligence*, vol. 7, Apr. 2024, Art. no. 1396160, https://doi.org/10.3389/frai.2024.1396160.

[29] C. Suedumrong, S. Phongmoo, T. Akarajaka, and K. Leksakul, "Diabetic Retinopathy Detection Using Convolutional Neural Networks with Background Removal, and Data Augmentation," *Applied Sciences*, vol. 14, no. 19, Sep. 2024, Art. no. 8823, https://doi.org/10.3390/app14198823.

[30] A. Jabbar *et al.*, "Deep Transfer Learning-Based Automated Diabetic Retinopathy Detection Using Retinal Fundus Images in Remote Areas," *International Journal of Computational Intelligence Systems*, vol. 17, no. 1, May 2024, Art. no. 135, https://doi.org/10.1007/s44196-024-00520-w.

[31] S. Devishri, B. Sangamitra, Y. Sakthivel, and K. Sujitha, "Diabetic Retinopathy Detection using Deep Learning," *International Journal of New Innovations in Engineering and Technology*, vol. 24, pp. 1591–1595, Mar. 2024, https://doi.org/10.1109/ICSTCEE49637.2020.9277506.

[32] A. M. Mutawa, K. Al-Sabti, S. Raizada, and S. Sruthi, "A Deep Learning Model for Detecting Diabetic Retinopathy Stages with Discrete Wavelet Transform," *Applied Sciences*, vol. 14, no. 11, May 2024, Art. no. 4428, https://doi.org/10.3390/app14114428.

[33] A. Rahman *et al.*, "Diabetic Retinopathy Detection: A Hybrid Intelligent Approach," *Computers, Materials & Continua*, vol. 80, no. 3, pp. 4561–4576, 2024, https://doi.org/10.32604/cmc.2024.055106.

[34] M. Gupta, "Target Detection by Fuzzy Gustafson-Kessel Algorithm," *International Journal of Image Processing*, vol. 7, no. 2, pp. 203–208, 2013.